Published in final edited form as:
Biomaterials. 2016 October ; 104: 168–181. doi:10.1016/j.biomaterials.2016.06.001.

Surface delivery of tunable doses of BMP-2 from an adaptable polymeric scaffold induces volumetric bone regeneration

Michael Bouyer[1,2,3], **Raphael Guillot**[1,2,$], **Jonathan. Lavaud**[4,5,$], **Cedric Plettinx**[1,2,#], **Cécile Olivier**[6,7,#], **Véronique Curry**[8], **Jean Boutonnat**[8,9], **Jean-Luc Coll**[4,5], **Françoise Peyrin**[6,7], **Véronique Josserand**[4,5], **Georges Bettega**[4,5,9,*], and **Catherine Picart**[1,2,*]

[1]CNRS, UMR 5628, LMGP, 3 parvis Louis Néel, F-38016 Grenoble, France

[2]Université de Grenoble Alpes, Grenoble Institute of Technology, 3 parvis Louis Néel, F-38016, Grenoble, France

[3]Service de chirurgie plastique et maxillo-faciale, Centre Hospitalier Universitaire de Grenoble, France

[4]INSERM U1209, Institut Albert Bonniot, F-38000 Grenoble, France

[5]Université Grenoble Alpes, Institut Albert Bonniot, F-38000 Grenoble, France

[6]Université de Lyon, CREATIS ; CNRS UMR5220 ; Inserm U1044 ; INSA-Lyon ; Université Claude Bernard Lyon 1, France

[7]ESRF, The European Synchrotron, CS 40220 38043 Grenoble, France

[8]Unité médico-technique d'Histologie Cytologie expérimentale, Faculté de Médecine, Université Joseph Fourier, 38700 La Tronche, France

[9]Département d'Anatomie et Cytologie Pathologique, Institut de biologie et de pathologie, Centre Hospitalier Universitaire de Grenoble, France

[10]Service de chirurgie maxillo-faciale, Centre Hospitalier Annecy Genevois, 1 avenue de l'hôpital –74370 Epagny Metz-Tessy, France

1 Introduction

The treatment of large bone defects resulting from trauma, non-union, tumor resections or craniofacial malformations remains challenging. More than 500,000 bone fractures require bone grafts in the USA among the 6.3 million annually reported cases and result in medical costs of $2.5 billion. [1] These conventional grafts, which combine osteogenic cells and osteoinductive and osteoconductive properties, [2, 3] are limited by donor-site morbidity, chronic inflammation or the risk of disease transmission. Synthetic bone scaffolds, such as osteoconductive ceramics [2] and biodegradable synthetic polymers, [4] have been developed to mimic bones, but they lack osteoinductive signals.

[*]Co-last and co-corresponding authors: gbettega@ch-annecygenevois.fr phone: +33(0)4 50 63 60 72, fax: +33(0)4 50 63 65 69; catherine.picart@grenoble-inp.fr, phone: +33(0)4 56 52 93 11, fax: +33(0)4 56 52 93 01.
[$]These authors have contributed equally (co-second authors)
[#]These authors have contributed equally (co-third authors)

Europe PMC Funders Author Manuscripts

Growth factors are particularly interesting because of their ability to target specific cellular receptors and actively trigger various cellular processes. [5] Among those involved in bone healing, bone morphogenetic protein (BMP)-2 is the most potent bone inductor [6] and is involved in different phases of repair. [7] BMP-2 has been used in orthopedic and maxillofacial surgery since 2003, [8] but its use has been paired solely with collagen as the only approved carrier. Unfortunately, the poor retention of BMP-2 by collagen leads to its rapid clearance from implantation sites, [9] and thus, supra-physiological doses (at least a few mg) are required. These issues have recently raised serious concerns regarding ectopic bone formation, pain and cancer risk. [10] Thus, there is a clear need to optimize the spatiotemporal delivery of BMPs using new carrier materials. [11]

BMPs may be delivered from two major strategies. The first consists in loading them in the “bulk” of space-filling materials, such as porous scaffolds, mostly ceramics [11, 12], biodegradable polymers [13] and hydrogels as carriers [14–16]. Indeed, natural polymers, polysaccharides and ECM proteins, such as hyaluronan, [17–19] heparin, [20, 21], fibronectin and fibrin, [22] are of interest because of their natural affinities for BMPs. They can be used to increase the retention of BMP-2 inside the bulk of the scaffolds [21] or for injectable formulations [18, 15]. For these space-filling composite materials, the release of BMP is intrinsically linked to the spatiotemporal degradation profile of the scaffold or hydrogel.

The second major strategy consists in functionalizing the surface of scaffolds to trap and subsequently release BMPs directly from the surface of scaffolds [23]. Surface coatings may potentially be applied to a variety of scaffolds of different shapes and chemical nature, including ceramics, metals, or synthetic polymers, thus broadening the potential for clinical applications of BMP-2 by adapting independently on one hand, the scaffold architecture and on the other hand, the BMP-2 dose delivered locally via the surface. To date, several methods have already been proposed to present BMP-2 at the surface of scaffolds either by direct grafting of BMP-2 [23] or by indirect adsorption via hydroxyapatite [24, 25] or biopolymers [26, 27, 20], thanks to their natural affinities with BMPs. However, direct grafting may be limited by the loss of BMP-2 bioactivity [23] and surface adsorption leads to low adsorbed doses of BMP-2. [26, 28]. Layer-by-layer films made of hydrolytically degradable polymers [29], polypeptides [30] or polysaccharides into which BMPs are adsorbed by physical interactions [31] constitute an interesting surface coating as their thickness can be easily tuned and they can act as a nano-reservoir for BMP-2 molecules. Recently, we have shown, using poly(L-lysine) (PLL) and hyaluronic acid (HA) polyelectrolyte films as a carrier for BMP-2 [31], that films deposited on ceramics and titanium implants are osteoinductive in a rat ectopic model [32, 33].

Here, our aim was to repair a volumetric (3D) bone defect, which was initially totally empty, by means of an osteoinductive polyelectrolyte multilayer film delivering tunable doses of BMP-2 from the surface (2D) of a film-coated PLGA scaffold. This cell-free approach for the repair of a large bone defect and is an “in-situ tissue engineering” approach, with the underlying ideas that i) the growth factors delivered by the surface coating will actively trigger the differentiation of precursor cells into bone cells and ii) the spatial localization of

the growth factors is provided by the underlying 3D polymeric scaffold and will guide the architecture of the subsequent tissue formation in the initially fully empty 3D scaffold.

We designed a 3D hollow tube in PLGA, a scaffold material widely used in maxillofacial surgeries [34] and orthopedics [35] that was custom-shaped to a critical-size femoral defect. By modulating the dose of BMP-2 in the film coating via the initial loading concentration of BMP-2 and the controlled crosslinking of the film, we showed that bone healing can be very fast (1-2 weeks) and maturation inside the PLGA hollow tube can be optimized from the absence of bone to excessive bone production. Importantly, a distinct spatial volumetric organization of bone was triggered by the BMP-2 film coating, with trabecular bone forming within the hollow tube and cortical bone forming around the scaffold, the thickness of the cortical being dependent on the BMP-2 dose.

2 Experimental Section

2.1 PLGA tube preparation and polyelectrolyte multilayer film (PEM) coating

0.25 mm thick 50 x 50 mm biodegradable Lactosorb sheets (Biomet Microfixation, Netherland), made of 82% poly(L-lactic) acid and 18% poly(glycolic) acid (PLGA, half-life = 6 months according to manufacturer data) were used for the *in vitro* and *in vivo* experiments. Before the film deposition, the planar sheets were trimmed and thermoformed at ~ 80°C into tubes to fit to 6 mm femoral defects (Fig. 1A). To this end, they were placed in an air active heat pack (Biomet Microfixation) for 10 to 15 s according to the manufacturer instructions. The surfaces of the PLGA tubes were measured to be 1.31 ± 0.05 cm^2 (means ± SEM).

The PEM film was deposited using 0.5-mg/mL poly(L-lysine) hydrobromide (PLL, 55 kDa, Sigma, France) and 1 mg/mL hyaluronic acid (HA, 360 kDa, Lifecore, USA).[33] The film crosslinking extent was controlled by incubating the coated tubes in 10-, 30-, or 70-mg/mL 1-ethyl-3-(3-dimethylaminopropyl)carbodiimide (EDC, Sigma, France) and 11-mg/mL N-hydroxysulfosuccinimide (sulfo-NHS, Sigma, France). BMP-2 was post-loaded in the PEM films at 5, 25, 50, or 100 μg/mL, as described previously [31]·[33]. Finally, the osteoinductive coated tubes were rinsed, dried, and stored at room temperature until implantation.

2.2 Characterization of PEM films and quantification of BMP-2 loading

Dry film thickness was measured by using a Dektak XT (Bruker Corporation) profilometer. Three samples $(PLL/HA)_{24}$ films deposited on silicon were scratched to create a physical step and three measurements per sample were acquired with the software Vision 64® (v 5.4, Bruker Corporation, USA). Scans of 30 s over a length of 1000 μm were performed with a stylus of 12.5 μm in radius and a force set to 1 mg. Thus, dry film thickness is an average value of 9 measurements.

The air dried PEM films coated on PLGA planar substrates were imaged by scanning electron microscopy (SEM) using a FEI-Quanta 250 SEM-FEG in high vacuum at 15 keV using the Everhart-Thornley detector.

The amounts of BMP-2 initially loaded into the PEM films and subsequently released after several washes with the Hepes-NaCl buffer were determined as previously described (1) by fluorescence spectrometry (TECAN Infinite 1000, Austria) using 5% of carboxyfluorescein labeled BMP-2 (BMP-2^{CF}) as a tracer. Knowing the total surface of the PLGA (see part 2.1), the total surface area of the PEM films was roughly estimated to be 2.6 cm^2, with the internal and external sides of the PLGA tubes being coated by the film. This value was used to convert the initial and final surface-adsorbed amounts, Γ_I and Γ_R (μg/cm^2), respectively, to absolute amounts (μg).

2.3 C2C12 cell culture and in vitro BMP-2 bioactivity assay

Murine C2C12 skeletal myoblasts (< 25 passages, obtained from the American Type Culture Collection, ATCC) were cultured in tissue culture Petri dishes. [32] The bioactivity of BMP-2 on C2C12 cells was determined by assaying the BMP-2 induced alkaline phosphatase (ALP) expression, which is an early marker of osteogenic differentiation. To this end, 90,000 cells in 1 mL of GM were seeded on each PLGA sample (square of 1 mm^2) in a 24-well plate. After 3 days of culture, the GM was removed and the cells were washed with PBS and lysed by sonication over 5 s in 500 mL of 0.1% Triton-X100 in PBS. The ALP activity of these lysates was then quantified using standard protocol [32] and normalized to the corresponding total protein content, which was determined using a bicinchoninic acid protein assay kit (Interchim, France).

2.4 In vivo critical-size defect in rat

All surgical procedures were reviewed and approved by the ethics committee in animal experimentation of Grenoble (Protocol 229_ IAB-U823-VJ-03). A 6 mm critical-size rat femoral defect model was chosen in this study because the non-healing nature of this model is well established [36, 37]. Female Wistar rats (Janvier, St Berthevin, France) aged 53 to 67 days were anesthetized using isoflurane and intraperitoneal injection of Ketamine Hydrochloride at 100 mg/kg body weight and medetomidine (Axience, Pantin, France) at 100 μg/kg body weight. All rats were operated on the right femur only. The rat was positioned in left lateral decubitus on a thermostatic heating plate to prevent hypothermia. The surgical area was shaved and scrubbed with povidone iodine. The incision was made on the anterolateral thigh, from the relief of the major trochanter to the knee. After the subcutaneous dissection, a longitudinal incision of the fascia lata muscle and a blunt dissection through the septum between the vastus lateralis and biceps femori were performed to expose the femur. A full-thickness diaphyseal critical-sized segmental defect of minimum 6 mm long was created using a circular mini-saw under irrigation. The periosteum was removed with the resected bone and on the remaining femoral fragments. The femur was stabilized by a titanium plate with a 12 mm bridge, and 4 screws of 1.7 mm in diameter (Stryker, France) associated with a distal and proximal 4/10 strapping steel wire (Nichrominox, Lyon, France). A PLGA tube was placed around the bone defect by overlapping to ~1 mm the femoral bone edges. These tubes were studded by a non-absorbable 4/0 suture. The wound was closed in a layered fashion by resorbable stitches. The rats carried a buster collar for 48 h. Animals were given 0.1 mg/kg buprenorphine subcutaneously every 12 h for the first 24 h post-surgery, and a tetracycline and trimethoprim sulfamethoxazole antibiotics for 48 h (Sigma-Aldrich, France). Within 2-3

postoperative days, the animals recovered a normal ambulation and did not show any sign of pain or distress.

First, in a preliminary experiment, we screened 10 conditions ($n = 2$) using X-ray before selecting 5 conditions that were further studied in larger groups ($n = 8$ at least for each) for statistical analysis (see Table 1 for all experimental conditions). Three controls were performed: i) defect left with no implant to confirm the critical size of the defect (no PLGA tube, $n = 3$), ii) bare PLGA ($n = 8$), iii) PLGA with BMP-2 directly adsorbed at 25 or 50 or 100 μg/mL on the PLGA tube (adsBMP-2, $n = 2$ for each concentration). Each implant was randomized, implanted and analyzed in a blind manner, the PEM films being macroscopically indistinguishable. All analyses of experimental groups were made in a blind manner. In the preliminary experiments, we noted that some rats presented clinical hematoma after the first 48 h post-surgery. In the subsequent experiments, during the first 48 hours, only rats that presented with a large clinical hematoma had a percutaneous puncture while those presenting with minimal clinical hematoma were not punctured, such assessment being made in a blind manner with respect to the experimental groups. After 8 weeks (56 days), the rats were euthanized by intracardiac injection of Dolethal (Vetoquinol, Paris, France) under gaseous anesthesia (isoflurane) and we reported the rats that had a clinical hematoma and rats that were punctured (Table 2). Plates and screws were then removed and the femurs were harvested fixed in 4% neutral buffered formalin (Sigma, France) for at least 24 h at 4°C.

2.5 Radiographic and μCT analysis using a commercial apparatus

Assessment of bone formation was made by X-ray after 0, 2, 4, 6 and 8 weeks. These radiographies were performed under gaseous anesthesia (isoflurane) on VivaCT 40 μCT (ScancoMedical, Brüttiselen, Switzerland) using scout views (55 kV, 300 ms).

An X-ray score was calculated in a blind manner by two surgeons analyzing the radiographies following the score proposed by Guldberg and coworkers [38]: (0) below half bone healing; (1) above half bone healing but still incomplete; (2) complete repair of the defect. The scores were fitted with an exponential function:

$$\text{X-ray score} = B_{max} \times [1 - \exp(-t/\tau)] \quad \text{eq (1)}$$

τ is the characteristic time of bone regeneration (in days) and B_{max} is the plateau value (in a.u.).

After 8 weeks, μCT imaging using this commercial apparatus (technique named hereafter CμCT) was performed on fixed bones using medium or high resolution scanner (70 kV, 114 mA, 42 μm isotropic voxel size). Sagittal cross sections and 3D representations were made using the Osirix© software. The volume of interest (VOI) was defined as the total volume of newly formed bone between the native bone ends. Contralateral femurs were used as internal controls for each rat with the same number of slices for the VOI concerned. The VOI was segmented by application of a global threshold (386 mg HA/cm^3) and a Gaussian filter

(sigma 0.8, support 1) to suppress the noise. Results were expressed as a bone volume ratio by dividing the newly formed bone volume by the volume of the internal control.

2.6 Histological analysis

The femurs were analyzed histologically after 8 weeks. After osteotomies of both epiphyses, the femurs were transferred to a 68% nitric acid-based decalcifier (VWR International, Basan, France) for 55 to 160 h depending on the bone hardness (felt with a surgical clamp). Following paraffin processing, 5 to 7 mm thick mid-sagittal sections were cut, pasted with albumin and stick-on (Labonord, Templemars, France) and stained with Safranin-O/Fast-green (Microm Microtech, Francheville, France), haematoxylin and eosin (Diapath, Martinengo, Italy). The histological slices were read in a blind manner by a pathologist, who attributed a score based on four criteria: (1) mesenchymal tissue, (2) ossification points (3) cancellous bone or (3) cortical bone. Thus the maximum total score was 9.

2.7 Synchrotron radiation micro-computed tomography (SRμCT)

The conditions that showed the best results in term of bone regeneration (kinetics of bone growth and bone volume) were further analyzed in greater detail using SRμCT at beamline ID19 at the European Synchrotron Radiation Facility (ESRF, Grenoble, France). Scans were performed with a 26.7 keV pink beam and setting the sample-detector distance at 400 mm enabling to record phase contrast. For each sample, 3800 projections were collected over a range of 360°. Images were reconstructed using Paganin's phase retrieval method [39] followed by the standard Filtered Back projection CT reconstruction algorithm. The Paganin method assumes proportionality between the linear attenuation coefficient (μ) proportional to the absorption index (β) and the refractive index decrement (δ), and the δ/β ratio was set to 430. The 3D reconstructed volume had an isotropic voxel size of $(3.5\ \mu m)^3$. The volume of interest (VOI) was determined in a similar fashion as described for the conventional μCT. The newly formed bone tissue was segmented by applying a global gray level threshold and two different bone tissues were clearly observed: cortical-like bone (Ct-bone) forming a compact shell of bone tissue outside the PLGA tube and trabecular-like bone (Tb-bone) forming a reticulated bone tissue mainly inside the PLGA tube. Ct-and Tb-bone were separately extracted based on their morphology using a segmentation workflow based on 3D region growing (software Avizo, FEI). 3D renderings showing the homogeneity of cortical bone and the trabecular network organization were obtained with the software VGStudio MAX (Volume Graphics GmbH).

Bone volume (BV) and total volume (TV) were determined for each VOI (i.e. Ct and Tb VOIs) by counting the number of non-zero pixels in binarized images and converting them to volumetric units (mm^3) using the voxel size. The mean thickness of bone structure was calculated by defining the 3D thickness at each point as the diameter of the largest sphere that can fit within the structure [40]. The connectivity of the trabecular network (β_1) was derived from the Euler number (χ) and was calculated automatically using an in-house program based on the method described by Odgaard [41]:

$$\beta_1 = \beta_0 + \beta_2 - \chi \quad \text{eq (2)}$$

where β_0 and β_2 respectively correspond to the number of connected components and cavities.

The density of connectivity (expressed in mm^{-3}) was then defined as β_1/TV where TV is the Total Volume as explained above.

These images were also used to quantify the mass density (ρ) within bone tissue thanks to the theoretical relationship linking the refractive index decrement to the mass density[42] :

$$\delta = 1.3 \cdot 10^6 \cdot \rho \cdot \lambda^2 \quad \text{eq (3)}$$

ρ (g/cm^3) corresponds to the mass density of the bone structure, λ (Å) corresponds to the selected wavelength of synchrotron radiation.

2.8 Statistics

Sigmaplot (Systat Software Inc) was used for all analyses. Non-parametric data were presented by median and interquartile range. Differences between groups were assessed by the Mann-Whitney U test for independent samples, with pairwise comparisons made by Bonferroni correction (multiple groups), and by the Wilcoxon paired test for paired samples. Parametric data were presented by mean and standard error of the mean (SEM). χ-squared analyses with individual comparisons were made by Fisher's exact test. A P value < 0.05 was considered significant.

3 Results

3.1 Tunable loading of bioactive BMP-2 in polyelectrolyte film-coated PLGA membranes

We used a commercially available Lactosorb® PLGA membrane trimmed and thermoformed at approximately 80°C into hollow 5 mm x 8 mm tubes to fit rat femoral defects (Figure 1). The PLGA tubes were coated with a PEM film made of 24 alternating layers of PLL and HA. Such (PLL/HA) films are known to growth exponentially with the number of deposited layer pairs from few tens of nanometers to several micrometers (hydrated thickness), which enable to modulate their thickness [43]. They contain a major amino-acid residue lysine, which bears amine groups and hyaluronan, which is a major component of the cellular coat [44] and of extracellular matrices [45]. As the concentration of the polyelectrolytes can influence film growth, we used previously established conditions for the film buildup (PLL at 0.5 mg/mL and HA at 1 mg/mL) [31].

The PEM film was crosslinked using tunable concentrations of 1-ethyl-3-(3-dimethylaminopropyl)carbodiimide (EDC) as a zero-length crosslinker. The films were named EDC10, EDC30, and EDC70 according to the crosslinker concentration used. Finally, the films were post-loaded with BMP-2 [31] at various concentrations ranging from 5 to 100 μg/mL In this previous study, we already proved that there is an interaction between HA and BMP-2 at pH 3 (acidic) and pH 7.4 (physiological) [31], which contribute to explain the observed high affinity of BMP-2 for the PEM films. Hereafter, the films are referred to as BMP5, BMP25, BMP50, and BMP100 to indicate the concentration of BMP-2 used. As

observed by scanning electron microscopy after scratching the film, the PEM film fully coated the PLGA surface (Figure 1A). Atomic force microscopy (in liquid) and profilometry (in the dry state) were used to measure the film cross-sections to quantify the hydrated and dry film thicknesses (6 μm ± 0.6 μm versus 870 ± 55 nm, respectively). Thus, the film thickness decreases by about 7 fold upon drying. For the *in vivo* study, the dry film-coated tubes were inserted into 6-mm long critical-size defects in rat femurs for 8 weeks (Figure 1B, C).

The amount of BMP-2 initially loaded into the PEM films and the percentage of released BMP-2 *in vitro* after several washes with a physiological (HEPES-NaCl) buffer were determined by fluorescent spectrometry using carboxyfluorescein-labelled BMP-2 ($BMP\text{-}2^{CF}$) as a tracer. [31] The total amount of BMP-2 loaded in the films (initial adsorbed amount Γ_i in μg) was dependent on the initial BMP-2 concentration in the loading solution and not on the EDC crosslinking (Figure 2A). Γ_i varied from 1.5 to 34.6 ± 0.8 μg as the BMP-2 concentration increased from 5 to 100 μg/mL. However, the percentage of released BMP-2 and the absolute released amounts (Γ_R) were dependent on the extent of crosslinking (Figure 2A, B). The release mostly occurred during the first 5 h and was higher for the EDC10 > EDC30 > EDC 70 (respectively 80 to 91%, 20 to 52% and 0 to 22%). Consequently, the Γ_R was consistently higher for the EDC10 films than the EDC30 and EDC70 films. Γ_R varied between 0 and 26.8 ± 0.8 μg depending on the extent of EDC crosslinking and BMP-2 dose. The bioactivity of the film-coated PLGA membranes was assessed using an ALP activity assay in C2C12 skeletal myoblasts (Figure 2C), an acknowledged cellular model to assess BMP-2 bioactivity *in vitro* [46]. The ALP activity increased in a dose-dependent manner and reached a plateau value for BMP25 doses, except for EDC10 films in which the ALP activity decreased at a BMP100 dose. The control ALP values for cells directly grown on the PLGA membranes when BMP-2 was delivered in solution (sBMP-2, 1.7 ± 0.1, blue line) or adsorbed (adsBMP-2, 0.9 ± 0.2, red line) on a bare PLGA membrane at the highest BMP-2 concentration (100 μg/mL) were systematically lower and similar to the activity of a film loaded at BMP5. We further verified the thermal molding of the PLGA tube after film deposition did not affect the bioactivity of the BMP-2-loaded PEM film (Figure S1).

3.2 BMP-2 dose influences the bone repair kinetics

The femoral critical-size defect in the rat is a well-established model [44] and was used here to test film-coated PLGA tubes. To optimize bone regeneration, we performed a preliminary experiment and initially screened in ten different conditions ($n = 2$), corresponding to four increasing concentrations of BMP-2 (BMP5, 25, 50, or 100) and three increasing crosslinking levels (EDC10, 30 and 70) (Table 1). Indeed, our previous data showed that the highest dose of BMP-2 (EDC10/BMP100) exhibited an osteoinductive capacity in a rat ectopic model. [32]

Conventional μCT (CμCT) acquisitions acquired 8 weeks after surgery enabled estimating the capacity of bone repair for the PEM coatings on PLGA tubes (Figure 3) and for the different control conditions (Figure S2). The negative control groups (empty defect; PLGA tube alone; and BMP-2 adsorbed at increasing concentrations on bare PLGA) showed no

callus or bone formation throughout the follow-up period (Figure S2 and Table 2). All BMP groups exhibited bone regeneration (Figure 3), whatever the crosslinking of the film, except the BMP5 group, which consistently showed very low bone regeneration without total healing of the defect. A continuous callus composed of “trabecular-like” bone (indicated by *) inside a thick “cortical-like” bone (indicated by a white arrow) was visible. For the EDC10/BMP100 group, hematomas appeared within 24 h after surgery and formed a calcified bony shell after 8 weeks.

We next repeated the experiments with more rats per condition (Table 1) to quantitatively assess the effects of BMP-2 concentrations (BMP25 to 100) and EDC crosslinking levels (EDC10 and EDC30) (Figure 4). We did not further studied the BMP5 groups because of their poor regenerative capacity. We also excluded the EDC70 groups because our previous data showed lower long-term film stability and an increased loss of bioactivity upon storage [33] than did the EDC10 and EDC30 films. Thus, in total, we continued with 5 experimental groups. The presence of clinical hematoma two day after surgery and the rats that required a percutaneous puncture were systematically noted and reported (Table 2). In Table 2, the percentage of bone healing is also systematically reported based on X-ray analysis. For the BMP25 group, bone healing was complete in 50 to 62.5% of the cases in comparison with 100% for BMP50 and BMP100. The BMP50 groups had hematomas in fewer than 12.5% of cases, whereas 75% of BMP100 samples presented hematomas. Their presence was significantly associated with the BMP100 condition ($P < 0.01$, Fisher test). Only BMP100 group showed large hematoma that required percutaneous puncture to avoid the formation of calcified bony shell like in the preliminary experiment. Others groups were not punctured and after 8 weeks no group showed calcified bony shell (Figure 4A and Table 2).

The ratio of newly formed bone relative to a reference volume of healthy bone was quantified at 8 weeks by CμCT (Figure 4B,C). The bone volume ratio increased with increasing BMP concentration, and the bone volume ratios for the BMP25, BMP50 and BMP100 groups were significantly different than the control group but were not significantly different among themselves. The EDC crosslinking level did not significantly influence the bone volume ratio because the BMP25 and BMP50 groups on EDC30 films exhibited levels similar to those of their EDC10 counterparts (Figure 4C).

The ratio of newly formed bone relative to a reference volume of healthy bone was quantified at 8 weeks by CμCT (Figure 4B). The bone volume ratio increased with increasing BMP concentration, and the bone volume ratios for the BMP25/EDC10, BMP50/EDC10, BMP50/EDC30 and BMP100/EDC10 groups were significantly different from the control group but were not significantly different among themselves (marked by #). The EDC crosslinking level did not significantly influence the bone volume ratio since the BMP25 and BMP50 groups on EDC30 films exhibited similar levels to those of their EDC10 counterparts. To note, the bone volume ratio for the BMP5/EDC10 and for the BMP25/EDC30 group was not significantly different from the control group (marked by NS). In addition, the BMP100/EDC10 group showed a significantly higher bone volume ratio than the BMP5/EDC10 and BMP25/EDC30 groups (marked by §) (Figure 4B).

To quantify the bone repair kinetics, an X-ray score was calculated for the EDC10 and EDC30 conditions based on X-ray images acquired every 2 weeks during the follow-up period (Figure 4C) This score was used to calculate a plateau value (B_{max}) and a characteristic bone-healing time scale (τ) by fitting an exponential function to the experimental data, for the conditions in which bone growth was observed. The scores steadily increased before reaching a plateau, $B_{max,}$ and were higher for the BMP50 and BMP100 groups. The characteristic time τ was approximately 3 times lower for the BMP50 (7.9 ± 0.4) and BMP100 groups (6.4 ± 0.9 days) than the BMP25 group (18 ± 2.3). Quantitatively similar kinetic curves were obtained for the EDC30 films loaded with the BMP25 and BMP50 doses, with B_{max} and τ values similar to those of the EDC10 (7.9 ± 0.3 for BMP50 and 15.4 ± 6.5 for BMP25, respectively, Figure 4C).

These data showed that the BMP-2 dose delivered from the PEM coating significantly influenced the repair kinetics of the bone defect and that this BMP-2 dose dependence was observed independently of EDC crosslinking levels.

3.3 Histological examination reveals the presence of maturing trabecular and cortical bones

A histological examination provided information on the repair process (Figure 5). There was no sign of foreign body reactions, as evidenced by the absence of inflammatory cells. The PLGA membrane (*T*) was still visible (its half-life is approximately 6 months). In the bare PLGA group, the tissue was characteristic of a non-union with abundant mesenchymal tissue (m) inside the tube and a few ossification points (o) without callus (Figure 5A). In the film-coated PLGA group (Figure 5B), there was a periosteal callus bridging the gap. The pattern was different between the outside and inside of the tube: a regenerated cortical (Ct) bone was observed outside and cancellous bone (Cn), and a small amount of mesenchymal tissue was found inside. Imaging at higher magnification outside the tube revealed that the cortical bone was approximately 200-400 μm thick with well-organized blood vessels (Figure 5C, D), showing that vascularization is present in the regenerated bone. On these sections, mineralized collagen strands and the PLGA tube were also clearly visible under polarized light (Figure 5C', 5D'). Inside the tube, normal trabeculae (Tb) with bone marrow (bm) between two cortical layers were present, similar to cancellous bone (Figure 5E). A few cells were in close contact with the surface of the film-coated PLGA tube (Figure 5F). The histological score, which was determined by a blinded pathologist, was significantly higher for the BMP-loaded films than the control PLGA group (Figure S3). Higher resolutions imaging inside cortical bone and mesenchymal tissue [47] revealed the presence of blood vessels inside the regenerated bone (Figure 6). The vessels can clearly be identified by the presence of red blood cells with a characteristic discoidal shape [48] in their lumen and of endothelial cells (ec, indicated by black arrows) lining along the vessel walls (Figure 6A, B). In addition, the imaging of PLGA with microscopy (Figure 6C) and polarized microscopy (Figure 6C'), where its surface is indicated by a red line, reveals its semi-crystalline structure by polarized microscopy. This dual observation also highlights a continuous thin line at its surface, which is only visible by microscopy (Figure 6C, **yellow arrows**) and not under polarized light (Figure 6C'). This line is indicative of the presence of the polyelectrolyte film coating at the PLGA surface (Figure 6C).

All observations were consistent with a lack of bone tissue in the control PLGA group and with maturing and vascularized new bone tissue in the case of the BMP-2-loaded films.

3.4 Spatial organization and BMP-2 dependence of bone formation revealed by synchrotron radiation μCT

Having demonstrated that bone regeneration occurred both inside and outside the PLGA tube, we next examined the spatial organization of bone tissue using high-resolution SRμCT (Figure 7). We pooled the BMP25 and BMP50 conditions, regardless of the EDC crosslinking level (10 and 30), because EDC did not have a major influence on bone repair (Figure 4). As a compact shell similar to cortical (Ct) bone was clearly observed outside the PLGA tube, whereas a reticulated bone tissue similar to trabecular (Tb) bone was mainly found inside the PLGA tube (Figure 7A), independently of the BMP-2 dose, we decided to segment the newly formed into distinct Ct and Tb bones. This was confirmed by the higher mass density of Ct than Tb bones (Figure 7B). Notably, after 8 weeks, this bone has formed everywhere inside the initially fully empty PLGA tube, even if BMP-2 was delivered at the tube surface. We observed that the Ct bone was more homogeneous along the length of the defect in the BMP50 group than in the BMP25 group (Figure 7A). The trabecular network was also more established inside the PLGA tube. Moreover, the total bone volume (i.e., the sum of the volumes of the Ct bone and the Tb bone) was higher for the BMP50 group ($P = 0.04$, Mann-Whitney U test, Figure 8A). In contrast, the amount of Tb bone did not significantly vary with the BMP-2 dose (Figure 8B). The increase in total bone volume was rather attributed to a significant increase in Ct-bone volume and Ct-thickness (Figure 8C,D). The connectivity of the Tb bone was not significantly different for the two groups (Figure 8E), but the Tb thickness decreased for the BMP50 group ($P = 0.13$, Mann-Whitney U test) (Figure 8F).

These data showed that the BMP-2 dose lead to spatially-distinct Tb and Ct bones and that the BMP-2 dose also had a significant influence on the Ct bone.

4 Discussion

Here, we showed that a volumetric critical size defect that was initially empty inside the PLGA tube can be repaired by the mere presence of an osteoinductive surface coating. Our data further showed the key role of the PEM film as a BMP-2 carrier because the bone-regeneration kinetics and the type of newly formed bone were dependent on the BMP-2 dose. The negative controls with bare PLGA, in the presence or absence of adsorbed BMP-2, showed the robustness of the rat femoral defect model (Figure 4 and S2). Here, the PLGA tube served as a physical and mechanical support scaffold for the osteoinductive film. We demonstrated that BMP-2 remained active after the thermal molding of PLGA (Figure S1), which indicates that, for future clinical applications, the film could first be deposited on the membrane before molding to the desired shape.

The novelty of the present study first resides in the combination of a 2D bioactive coating, which can deliver tunable doses of BMP-2, with a 3D scaffold, which provide the necessary template for the film. Second, it resides in the fact that we bring here new experimental results showing the capacity of the 2D film/3D hollow scaffold to repair a critical-size bone

femoral defect, with the formation of vascularized cortical and cancellous bone inside the initially empty scaffold and at its surface. Basically, a new bone is formed in an initially fully-empty space with solely a hollow tube as *initial* mechanical support. In addition, we showed that the quality and amount of bone formed depends on the dose of BMP-2 delivered by the 2D surface coating.

We adapted the BMP-2 dose delivered from the PEM surface coating by varying the BMP-2 loading concentration and the EDC crosslinking level. The initial loading amounts in the films were tuned by controlling the BMP-2 concentrations, whereas the release profiles were modulated via the extent of crosslinking (Figure 2). In our previous study, we already proved that there is an interaction between HA and BMP-2 both at pH 3 (acidic conditions) and at pH 7.4 (physiological conditions) [31], which contribute to explain the observed high affinity of BMP-2 for the PEM films. Film crosslinking is expected to modulate film nanometer scale porosity, a more crosslinked thus interconnected network having smaller pore size. Thus, the increased level of film crosslinking is consistent with the observed decrease in BMP-2 release (EDC10>EDC30>EDC70 in terms of released amount). Regarding the underlying mechanism driving BMP-2 release from the film in vivo, we may draw some hypothesis. The hydrated and dry film thicknesses are 6 μm ± 0.6 μm versus 870 ± 55 nm, respectively, which corresponds to a 7 fold decrease in thickness upon drying of the film (i.e. the film shrinks). Thus, one may anticipate that a “sponge” effect is occurring upon implantation of the dry film-coated scaffold and contact with biological fluids. The rehydration will induce film swelling and, consequently, BMP-2 release. Here again, low crosslinked films (EDC10) are expected to release more BMP-2. Second, in view of the nature of PLL and HA as biopolymeric components of the films and the presence of various enzymes in vivo, including hyaluronidase [49], we anticipate that the film should be biodegradable. Here again, a less crosslinked network should be more easily degradable, which was already shown to be the case for crosslinked chitosan/HA films [50]. Thus, we may hypothesize two different and complementary mechanisms for BMP-2 release: i) first, a release due to the initial film-swelling; and ii) second on a longer-term, a release associated to film biodegradability. Technically, film biodegradability in vivo is extremely challenging to assess in view of the roughness of PLGA, the micrometer thickness of the hydrated film (Figure 6), and the poor contrast of the film and PLGA. Indeed, SEM images in vitro (e.g. in easier imaging conditions) enabled to reveal the presence of the film only after scratching it (Figure 1) and in vivo histological imaging revealed, at the micron scale, that the film is still at present at the PLGA surface after 2 months but cannot be used to investigate its nanometer scale biodegradability.

We showed that the kinetics of bone regeneration and the volume of newly formed bone depended on the delivered dose of BMP-2 (Figure 3 and 4). However, an excessive BMP-2 dose (BMP100) was associated with the presence of large hematomas and if not punctured, calcified shell formation. For lower BMP-2 doses, only minimal clinical hematoma could occur (one rat out of 8) but these were spontaneously resorbed and did not lead to calcified shell formation. Our data are in agreement with previous studies using approved collagen sponges BMP-2 delivery systems, [51–53] with the occurrence of encapsulated hematomas at high doses of BMP-2[51] and with our recent data of transient bone loss around film-

coated titanium and poly(etheretherketone) screws (with the dose EDC10/BMP100) implanted in the rabbit femoral condyle [54].

Based on the amounts of BMP-2 incorporated in the films (Figure 2) and on our results that show bone formation between BMP25 and BMP50 irrespective of EDC crosslinking (Figure 3, 4 and Table 2), we can estimate the minimal BMP dose required to induce complete repair of the femoral bone defect. These thresholds are between the highest released amount (6.5 μg) for the BMP25 group (corresponding to EDC10/BMP25) and the lowest released amount (7.8 μg) for the BMP50 groups (corresponding to EDC30/BMP50) (Figure 2). The BMP-2 concentration in the loading solution amount was found to be more influential on the bone volume and growth kinetics than the EDC crosslinking (Figure 4), highlighting the greater role of the initial total loaded of amount BMP-2 (Γ_i), which is globally similar for all EDC conditions, in comparison to the initially released amount (% rel and Γ_R), which is mostly dependent on the EDC crosslinking level (Figure 2). Importantly, the kinetics of bone regeneration depended on the BMP-2 dose and was extremely rapid for BMP50 and 100 with τ of 7 days (Figure 4).

To the best of our knowledge, only one study by Guldberg *et al.,*[14] who used a similar femoral defect model, has focused on the influence of the BMP-2 dose delivered from a porous polycaprolactone tube filled with an alginate gel as the BMP-2 carrier. Thus, the gel was filling the entire volume of the tube and was not a surface coating. By testing six doses from 0 to 5 μg, they found that bone volume and connectivity were not linearly correlated with the BMP-2 dose and further observed a reduced response beyond 1.0 μg for alginate and a different dose response for the collagen sponge. In their study, bone slowly formed with continued growth for 8 and 12 weeks [14] and the kinetics of bone growth was independent of the BMP-2 dose. The differences in the kinetics and BMP-2 dose response between their study and ours may be due to the different BMP-2 presentations: in the bulk of the alginate gel filling a porous tube [14] versus direct delivery by the surface of a hollow tube in our study.

Using a similar approach of composite scaffold, made of porous polypropylene fumarate (PPF) incorporating gelatin micro-particles (GMP), which are crosslinked with glutaraldehyde and serve as carriers for VEGF and BMP-2 release, Mikos *et al.* [55] studied the combined influence of BMP-2 and VEGF on bone repair in a rat calvarial defect. They found a dose-dependent decrease in bone repair with the BMP-2 dose, which could not be reversed by the addition of VEGF. It is interesting to note that, in a system where BMP-2 and VEGF release are intrinsically linked to the biodegradability of the composite carrier (GMP and PPF), the addition of a second growth factor (VEGF) did not improve the repair process. This highlights the interest for optimizing simple systems (i.e. less components) and not necessary adding complexity in a system.

Regarding surface coatings, Hammond *et al.* [56] recently studied the regenerative capacity of hydrolyzable PEM coatings loaded at two BMP-2 doses (0.2 and 2 μg) deposited on circular and planar PLGA membranes in a rat calvarial bone defect model. The calvarial defect can considered as a “surfacic“ and planar bone defect and, because of the proximity of dura mater providing stem cells and growth factors, was found to enable bone repair after

8 weeks, even in the absence of growth factors [53]. In this model, there was no significant difference between two BMP-2 doses or when PDGF was co-delivered with BMP-2 [56] but alendronate added as a supplementary ingredient improved rate and quality of bone repair. PEM coating with two active ingredients [56], similarly to hydrogels that deliver two active growth factors [57], showed improved bone regeneration capacities but may be more difficult to translate clinically. In fact, clinical translation requires that all components of the final drug will want quantifying in vivo in urine and feces to show effective half-life and clearance [58].

Our CT data and histological observations (Figures 4-8) showed that after 8 weeks, the newly formed bone was in a matured state composed of both cortical and trabecular bones with blood vessels and mineralized collagen. Vascularization plays a critical role in bone function and repair [59] because it permits communication between cells and the mineralization of the extracellular matrix. The lower mass density of Tb bone calculated from all samples (Figure 6B) was in line with reported increased, metabolically active states with Tb remodeling [60]. The spatial 3D organization of the bone tissue was likely facilitated by the empty PLGA tube, which provided a 3D space for bone regeneration both inside and outside the tube. Indeed, he the mass density of Ct-bone was higher for Tb (Figure 6B), and cortical thickness of the BMP50 group was great than that of BMP25 (Figure 7C). However, these measurements were not directly observed in the current study. Although the connectivity values were not different, the trabecular bone was thinner for the BMP50 group (Figure 7E). We hypothesize that over time and under the influence of mechanical stimulus, trabeculae may disappear to form normal diaphyseal bone devoid of trabecular bone and become essentially composed of thick cortical bone.

In the context of this regenerated volumetric bone defect, what about the potential biodegradation of the supporting PLGA scaffold itself? According to the technical datasheet provided by the manufacturer, the half-life of Lactosorb is 6 month [61]. Biodegradation occurs by hydrolysis. At 2 months (our time point), 95 % of it mass and 70% of its strength are remaining. In vitro data indicate that, after 33 days of exposure to buffer, there was no change in physical appearance, dimensions or shape of Lactosorb screws [62]. Strength loss profiles also demonstrated peak strength retention (flexural and shear) for about 8 weeks [63]. In vivo, no change in shape of Lactosorb plates and screws was seen and a non-inflammatory layer of surrounding fibrous tissue was present [64], the safety and benefits of this material being confirmed on the long-term [35]. Our histological observations and SRμCT images are consistent with these previous results as the PLGA tube is clearly still present, with cells in contact with it (Figure 4) and with no sign of biodegradation (Figure 6, PLGA tube visible by birefringence microscopy and Figure 7- tube visible in gray color by SR-μCT). It is also clear that PLGA is coated with the film (Figure 6) and that bone is in contact with the 3D hollow tube (Figure 5). Indeed, the presence of the polyelectrolyte film and bone may affect the hydrolysis rate of PLGA and rather protect is from biodegradation. Having this information in mind, we may anticipate that it would take at least about a year for the PLGA to biodegrade. In this timeframe, the regenerated bone would have been sufficiently formed and may not need any more a mechanical support, in contrast to the initial time upon implantation where this was needed for the film and initial anchor of bone growth.

Altogether, our results show that it is the appropriate choice of the 3D scaffold architecture in combination with the 2D bioactive coatings that enables this impressive and tunable bone repair. The PEM film coating presented herein has several technological advantages that show promise for clinical applications and approval by regulatory agencies.

One key advantage of our approach is that both the dose of BMP-2 delivered by the film-coating (2D) and the architecture or type of 3D scaffolds (3D) can be modulated and adapted independently of each other. A potential disadvantage of the 2D film-coating is that it needs to be associated with a 3D scaffold and is not “free-standing”. Thus, the scaffold design itself should first be optimized before the film coating can be applied.

The film is made by a simple self-assembly of biopolymers and contained only one growth factor, BMP-2. The film can be dried, stored off-the-shelf and sterilized by γ-irradiation, [33] which is a commonly used sterilization method for orthopedic implants. Finally, HA, EDC and BMP-2 are components approved by the US Food and Drug Administration (FDA) and the European Medicine Agencies (EMA) for bone tissue engineering and the crosslinking of collagen matrices. PLL has also been approved for food applications. Last but not least, thanks to the film tunability, the BMP-2 dose may be modulated depending on the need (in vivo localization of the bone defect and its size).

In view of the possibility to apply the film on a large variety of 3D volumetric scaffolds, it may be envisioned to combine the films with different types of polymers or metallic alloy commonly used in orthopedics, maxillofacial surgery, dentistry or veterinary medicine. Or particular interest are the recent developments in additive manufacturing techniques [65, 66], which have shown their broad applicability to polymers such as polycaprolactone [12] or to metallic alloy such as titanium [67]. The unprecedented potentialities offered by these innovative techniques to create a large variety of scaffold shapes and architectures, combined with the new possibility to optimize the BMP-2 dose open new perspectives for personalized medicine. As our first proof of concept, we selected here the commercially-available Lactosorb PLGA sheet as a polymeric scaffold, since Lactosorb it is already widely used in clinics. Since we have already proved the possibility to coat TCP/HAP granules [32] and titanium scaffolds [33] with the BMP-2 loaded films, which were also shown to induce ectopic bone growth, we foresee that ceramics and titanium scaffold could also be, in a near future, combined with the osteoinductive coatings to repair volumetric bone defects [68].

Our technology provides an alternative to conventional bone grafts for the targeted repair of large bone defects using bioactive PEM 2D surface coatings of 3D volumetric scaffolds. The next step in view of its pre-clinical validation and clinical translation will undoubtedly to prove its efficacy in a larger animal model.

Conclusions

Using a polyelectrolyte film loaded with tunable doses of BMP-2 as osteoinductive surface coating of a hollow PLGA tube, which was initially fully empty, we show that the repair of a bone volumetric defect is dependent on the amount of BMP-2 released by the polyelectrolyte film coating. Depending on the BMP-2 dose, a range of responses, from no

effect to rapid bone repair in 1 week, can be achieved, including complete defect bridging and the formation of vascularized and mineralized bone tissue. High-resolution computed tomography revealed the presence of bone regeneration inside and around the tube with spatially distinct organization for trabecular-like and cortical bone. This efficient way to trigger a fast volumetric bone regeneration via the surface of an implant opens perspectives for applications of these coatings in personalized medicine. The simplicity and robustness of the present coating is an advantage for its broad applicability for other bone repair applications, since the bioactive surface coating can be adapted to different types of materials (polymers, ceramics, metals) of any topology, including architectured materials.

Supplementary Material

Refer to Web version on PubMed Central for supplementary material.

Acknowledgements

This work was supported by the “Association Gueules Cassées” (contract no. 322013 to GB) and by the European Commission under the FP7 program (European Research Council grant BIOMIM GA 259370 and Proof of Concept OSCODI GA334966 and to C.P.). Bone imaging systems were acquired thanks to France Life Imaging (FLI, French program “Investissement d’Avenir”; grant “Infrastructure d’avenir en Biologie Santé”, ANR-11-INBS-44 0006). Max Langer and Loriane Weber are acknowledged for their technical help with the ESRF experiments and Céline Genty for her help with the statistical analysis. We are grateful to Thomas Crouzier and Thomas Boudou for their useful comments on the manuscript.

References

[1]. Laurencin C, Khan Y, El-Amin SF. Bone graft substitutes. Expert review of medical devices. 2006; 3:49–57. [PubMed: 16359252]

[2]. Giannoudis PV, Dinopoulos H, Tsiridis E. Bone substitutes: an update. Injury. 2005; 36(Suppl 3):S20–7. [PubMed: 16188545]

[3]. Janicki P, Schmidmaier G. What should be the characteristics of the ideal bone graft substitute? Combining scaffolds with growth factors and/or stem cells. Injury. 2011; 42(Suppl 2):S77–81. [PubMed: 21724186]

[4]. Puppi D, Chiellini F, Piras AM, Chiellini E. Polymeric materials for bone and cartilage repair. Prog Polym Sci. 2010; 35:403–440.

[5]. Lee K, Silva EA, Mooney DJ. Growth factor delivery-based tissue engineering: general approaches and a review of recent developments. J R Soc Interface. 2011; 8:153–70. [PubMed: 20719768]

[6]. Urist MR. Bone - formation by autoinduction. Science. 1965; 150:893. [PubMed: 5319761]

[7]. Santo VE, Gomes ME, Mano JF, Reis RL. Controlled release strategies for bone, cartilage, and osteochondral engineering--Part I: recapitulation of native tissue healing and variables for the design of delivery systems. Tissue Eng Part B Rev. 2013; 19:308–26. [PubMed: 23268651]

[8]. Schmidmaier G, Schwabe P, Strobel C, Wildemann B. Carrier systems and application of growth factors in orthopaedics. Injury. 2008; 39(Suppl 2):S37–43.

[9]. Geiger M, Li RH, Friess W. Collagen sponges for bone regeneration with rhBMP-2. Adv Drug Deliv Rev. 2003; 55:1613–29. [PubMed: 14623404]

[10]. Carragee EJ, Hurwitz EL, Weiner BK. A critical review of recombinant human bone morphogenetic protein-2 trials in spinal surgery: emerging safety concerns and lessons learned. Spine J. 2011; 11:471–91. [PubMed: 21729796]

[11]. Lo KWH, Ulery BD, Ashe KM, Laurencin CT. Studies of bone morphogenetic protein-based surgical repair. Adv Drug Deliv Rev. 2012; 64:1277–1291. [PubMed: 22512928]

[12]. Reichert JC, Cipitria A, Epari DR, Saifzadeh S, Krishnakanth P, Berner A, et al. A tissue engineering solution for segmental defect regeneration in load-bearing long bones. Sci Transl Med. 2012; 4:141ra93.

[13]. Saito N, Takaoka K. New synthetic biodegradable polymers as BMP carriers for bone tissue engineering. Biomaterials. 2003; 24:2287–93. [PubMed: 12699665]

[14]. Boerckel JD, Kolambkar YM, Dupont KM, Uhrig BA, Phelps EA, Stevens HY, et al. Effects of protein dose and delivery system on BMP-mediated bone regeneration. Biomaterials. 2011; 32:5241–51. [PubMed: 21507479]

[15]. Bhakta G, Rai B, Lim ZX, Hui JH, Stein GS, van Wijnen AJ, et al. Hyaluronic acid-based hydrogels functionalized with heparin that support controlled release of bioactive BMP-2. Biomaterials. 2012; 33:6113–22. [PubMed: 22687758]

[16]. Martino MM, Briquez PS, Maruyama K, Hubbell JA. Extracellular matrix-inspired growth factor delivery systems for bone regeneration. Adv Drug Deliv Rev. 2015; 94:41–52. [PubMed: 25895621]

[17]. Kim HD, Valentini RF. Retention and activity of BMP-2 in hyaluronic acid-based scaffolds in vitro. J Biomed Mater Res. 2002; 59:573–84. [PubMed: 11774316]

[18]. Martinez-Sanz E, Ossipov DA, Hilborn J, Larsson S, Jonsson KB, Varghese OP. Bone reservoir: Injectable hyaluronic acid hydrogel for minimal invasive bone augmentation. J Control Release. 2011; 152:232–40. [PubMed: 21315118]

[19]. Kisiel M, Martino MM, Ventura M, Hubbell JA, Hilborn J, Ossipov DA. Improving the osteogenic potential of BMP-2 with hyaluronic acid hydrogel modified with integrin-specific fibronectin fragment. Biomaterials. 2013; 34:704–12. [PubMed: 23103154]

[20]. Belair DG, Le NN, Murphy WL. Design of growth factor sequestering biomaterials. Chem Commun (Camb). 2014; 50:15651–68. [PubMed: 25182455]

[21]. Ma C, Jing Y, Sun H, Liu X. Hierarchical Nanofibrous Microspheres with Controlled Growth Factor Delivery for Bone Regeneration. Adv Healthc Mater. 2015; 4:2699–708. [PubMed: 26462137]

[22]. Martino MM, Tortelli F, Mochizuki M, Traub S, Ben-David D, Kuhn GA, et al. Engineering the growth factor microenvironment with fibronectin domains to promote wound and bone tissue healing. Sci Transl Med. 2011; 3:100ra89.

[23]. King WJ, Krebsbach PH. Growth factor delivery: how surface interactions modulate release in vitro and in vivo. Adv Drug Deliv Rev. 2012; 64:1239–56. [PubMed: 22433783]

[24]. Liu Y, Enggist L, Kuffer AF, Buser D, Hunziker EB. The influence of BMP-2 and its mode of delivery on the osteoconductivity of implant surfaces during the early phase of osseointegration. Biomaterials. 2007; 28:2677–86. [PubMed: 17321590]

[25]. Suarez-Gonzalez D, Lee JS, Diggs A, Lu Y, Nemke B, Markel M, et al. Controlled multiple growth factor delivery from bone tissue engineering scaffolds via designed affinity. Tissue Eng Part A. 2014; 20:2077–87. [PubMed: 24350567]

[26]. Schliephake H, Aref A, Scharnweber D, Bierbaum S, Roessler S, Sewing A. Effect of immobilized bone morphogenic protein 2 coating of titanium implants on peri-implant bone formation. Clin Oral Implants Res. 2005; 16:563–9. [PubMed: 16164462]

[27]. Abarrategi A, Moreno-Vicente C, Ramos V, Aranaz I, Sanz Casado JV, Lopez-Lacomba JL. Improvement of porous beta-TCP scaffolds with rhBMP-2 chitosan carrier film for bone tissue application. Tissue Eng Part A. 2008; 14:1305–19. [PubMed: 18491953]

[28]. Kim SE, Song SH, Yun YP, Choi BJ, Kwon IK, Bae MS, et al. The effect of immobilization of heparin and bone morphogenic protein-2 (BMP-2) to titanium surfaces on inflammation and osteoblast function. Biomaterials. 2011; 32:366–73. [PubMed: 20880582]

[29]. Shah NJ, Hong J, Hyder MN, Hammond PT. Osteophilic multilayer coatings for accelerated bone tissue growth. Adv Mater. 2012; 24:1445–50. [PubMed: 22311551]

[30]. Dierich A, Le Guen E, Messaddeq N, Stoltz S, Netter P, Schaaf P, et al. Bone formation mediated by synergy-acting growth factors embedded in a polyelectrolyte multilayer film. Advanced Materials. 2007; 19:693–697.

[31]. Crouzier T, Ren K, Nicolas C, Roy C, Picart C. Layer-by-Layer films as a biomimetic reservoir for rhBMP-2 delivery: controlled differentiation of myoblasts to osteoblasts. Small. 2009; 5:598–608. [PubMed: 19219837]

[32]. Crouzier T, Sailhan F, Becquart P, Guillot R, Logeart-Avramoglou D, Picart C. The performance of BMP-2 loaded TCP/HAP porous ceramics with a polyelectrolyte multilayer film coating. Biomaterials. 2011; 32:7543–54. [PubMed: 21783243]

[33]. Guillot R, Gilde F, Becquart P, Sailhan F, Lapeyrere A, Logeart-Avramoglou D, et al. The stability of BMP loaded polyelectrolyte multilayer coatings on titanium. Biomaterials. 2013; 34:5737–46. [PubMed: 23642539]

[34]. Enislidis G, Pichorner S, Kainberger F, Ewers R. Lactosorb panel and screws for repair of large orbital floor defects. J Craniomaxillofac Surg. 1997; 25:316–21. [PubMed: 9504308]

[35]. Eppley BL, Morales L, Wood R, Pensler J, Goldstein J, Havlik RJ, et al. Resorbable PLLA-PGA plate and screw fixation in pediatric craniofacial surgery: clinical experience in 1883 patients. Plast Reconstr Surg. 2004; 114:850–6. discussion 857. [PubMed: 15468389]

[36]. Brown KV, Li B, Guda T, Perrien DS, Guelcher SA, Wenke JC. Improving bone formation in a rat femur segmental defect by controlling bone morphogenetic protein-2 release. Tissue Eng Part A. 2011; 17:1735–46. [PubMed: 21338268]

[37]. Sato K, Watanabe Y, Harada N, Abe S, Matsushita T, Yamanaka K, et al. Establishment of reproducible, critical-sized, femoral segmental bone defects in rats. Tissue Eng Part C Methods. 2014; 20:1037–41. [PubMed: 24738624]

[38]. Shekaran A, Garcia JR, Clark AY, Kavanaugh TE, Lin AS, Guldberg RE, et al. Bone regeneration using an alpha 2 beta 1 integrin-specific hydrogel as a BMP-2 delivery vehicle. Biomaterials. 2014; 35:5453–61. [PubMed: 24726536]

[39]. Paganin D, Mayo SC, Gureyev TE, Miller PR, Wilkins SW. Simultaneous phase and amplitude extraction from a single defocused image of a homogeneous object. J Microsc. 2002; 206:33–40. [PubMed: 12000561]

[40]. Bonnassie A, Peyrin F, Attali D. A new method for analyzing local shape in three-dimensional images based on medial axis transformation. IEEE transactions on systems, man, and cybernetics. Part B, Cybernetics : a publication of the IEEE Systems, Man, and Cybernetics Society. 2003; 33:700–5.

[41]. Odgaard A, Gundersen HJ. Quantification of connectivity in cancellous bone, with special emphasis on 3-D reconstructions. Bone. 1993; 14:173–82. [PubMed: 8334036]

[42]. Langer M, Pacureanu A, Suhonen H, Grimal Q, Cloetens P, Peyrin F. X-ray phase nanotomography resolves the 3D human bone ultrastructure. PLoS One. 2012; 7:e35691. [PubMed: 22952569]

[43]. Picart C, Mutterer J, Richert L, Luo Y, Prestwich GD, Schaaf P, et al. Molecular basis for the explanation of the exponential growth of polyelectrolyte multilayers. Proc Natl Acad Sci USA. 2002; 99:12531–12535. [PubMed: 12237412]

[44]. Zaidel-Bar R, Cohen M, Addadi L, Geiger B. Hierarchical assembly of cell-matrix adhesion complexes. Biochem Soc Trans. 2004; 32:416–420. [PubMed: 15157150]

[45]. Laurent TC, Laurent UB, Fraser JR. Functions of hyaluronan. Ann Rheum Dis. 1995; 54:429–32. [PubMed: 7794055]

[46]. Katagiri T, Yamaguchi A, Komaki M, Abe E, Takahashi N, Ikeda T, et al. Bone morphogenetic protein-2 converts the differentiation pathway of C2C12 myoblasts into the osteoblast lineage. J Cell Biol. 1994; 127:1755–66. [PubMed: 7798324]

[47]. Travlos GS. Normal structure, function, and histology of the bone marrow. Toxicol Pathol. 2006; 34:548–65. [PubMed: 17067943]

[48]. Picart C, Carpentier PH, Galliard H, Piau J-M. Blood yield stress in systemic sclerosis. Am J Physiol. 1999; 276:H771–H777. [PubMed: 9950881]

[49]. Laurent, TC. The chemistry, biology, and medical applications of hyaluronan and its derivatives. Cambridge University Press; Cambridge, U.K: 1998.

[50]. Picart C, Schneider A, Etienne O, Mutterer J, Egles C, Jessel N, et al. Controlled degradability of polysaccharides multilayer films in vitro and in vivo. Adv Funct Mat. 2005; 15:1771–1780.

[51]. Lee KB, Taghavi CE, Song KJ, Sintuu C, Yoo JH, Keorochana G, et al. Inflammatory characteristics of rhBMP-2 in vitro and in an in vivo rodent model. Spine (Phila Pa 1976). 2011; 36:E149–54. [PubMed: 21242879]

[52]. Zara JN, Siu RK, Zhang X, Shen J, Ngo R, Lee M, et al. High doses of bone morphogenetic protein 2 induce structurally abnormal bone and inflammation in vivo. Tissue Eng Part A. 2011; 17:1389–99. [PubMed: 21247344]

[53]. Pelaez M, Susin C, Lee J, Fiorini T, Bisch FC, Dixon DR, et al. Effect of rhBMP-2 dose on bone formation/maturation in a rat critical-size calvarial defect model. J Clin Periodontol. 2014; 41:827–36. [PubMed: 24807100]

[54]. Guillot R, Pignot-Paintrand I, Lavaud J, Decambron A, Bourgeois E, Josserand V, et al. Assessment of a polyelectrolyte multilayer film coating loaded with BMP-2 on titanium and PEEK implants in the rabbit femoral condyle. Acta Biomater. 2016

[55]. Young S, Patel ZS, Kretlow JD, Murphy MB, Mountziaris PM, Baggett LS, et al. Dose effect of dual delivery of vascular endothelial growth factor and bone morphogenetic protein-2 on bone regeneration in a rat critical-size defect model. Tissue Eng Part A. 2009; 15:2347–62. [PubMed: 19249918]

[56]. Shah NJ, Hyder MN, Quadir MA, Dorval Courchesne NM, Seeherman HJ, Nevins M, et al. Adaptive growth factor delivery from a polyelectrolyte coating promotes synergistic bone tissue repair and reconstruction. Proc Natl Acad Sci U S A. 2014; 111:12847–52. [PubMed: 25136093]

[57]. Ratanavaraporn J, Furuya H, Kohara H, Tabata Y. Synergistic effects of the dual release of stromal cell-derived factor-1 and bone morphogenetic protein-2 from hydrogels on bone regeneration. Biomaterials. 2011; 32:2797–811. [PubMed: 21257197]

[58]. Eaton MA, Levy L, Fontaine OM. Delivering nanomedicines to patients: a practical guide. Nanomedicine : nanotechnology, biology, and medicine. 2015; 11:983–92.

[59]. Krishnan L, Willett NJ, Guldberg RE. Vascularization strategies for bone regeneration. Ann Biomed Eng. 2014; 42:432–44. [PubMed: 24468975]

[60]. Rho JY, Kuhn-Spearing L, Zioupos P. Mechanical properties and the hierarchical structure of bone. Med Eng Phys. 1998; 20:92–102. [PubMed: 9679227]

[61]. Biomet.de, LactoSorb Distraction. 2008

[62]. Pietrzak WS, Eppley BL. In vitro characteristics of a bioabsorbable suspension screw and suture system for endoscopic brow lift surgery. J Craniofac Surg. 2007; 18:429–36. [PubMed: 17414297]

[63]. Pietrzak WS, Caminear DS, Perns SV. Mechanical characteristics of an absorbable copolymer internal fixation pin. The Journal of foot and ankle surgery : official publication of the American College of Foot and Ankle Surgeons. 2002; 41:379–88.

[64]. Eppley BL, Reilly M. Degradation characteristics of PLLA-PGA bone fixation devices. J Craniofac Surg. 1997; 8:116–20. [PubMed: 10332278]

[65]. Giannitelli SM, Mozetic P, Trombetta M, Rainer A. Combined additive manufacturing approaches in tissue engineering. Acta Biomater. 2015; 24:1–11. [PubMed: 26134665]

[66]. Tang D, Tare RS, Yang LY, Williams DF, Ou KL, Oreffo ROC. Biofabrication of bone tissue: approaches, challenges and translation for bone regeneration. Biomaterials. 2016; 83:363–382. [PubMed: 26803405]

[67]. Yavari SA, van der Stok J, Chai YC, Wauthle R, Birgani ZT, Habibovic P, et al. Bone regeneration performance of surface-treated porous titanium. Biomaterials. 2014; 35:6172–6181. [PubMed: 24811260]

[68]. Farre-Guasch E, Wolff J, Helder MN, Schulten EA, Forouzanfar T, Klein-Nulend J. Application of Additive Manufacturing in Oral and Maxillofacial Surgery. J Oral Maxillofac Surg. 2015; 73:2408–18. [PubMed: 25966454]

Europe PMC Funders Author Manuscripts

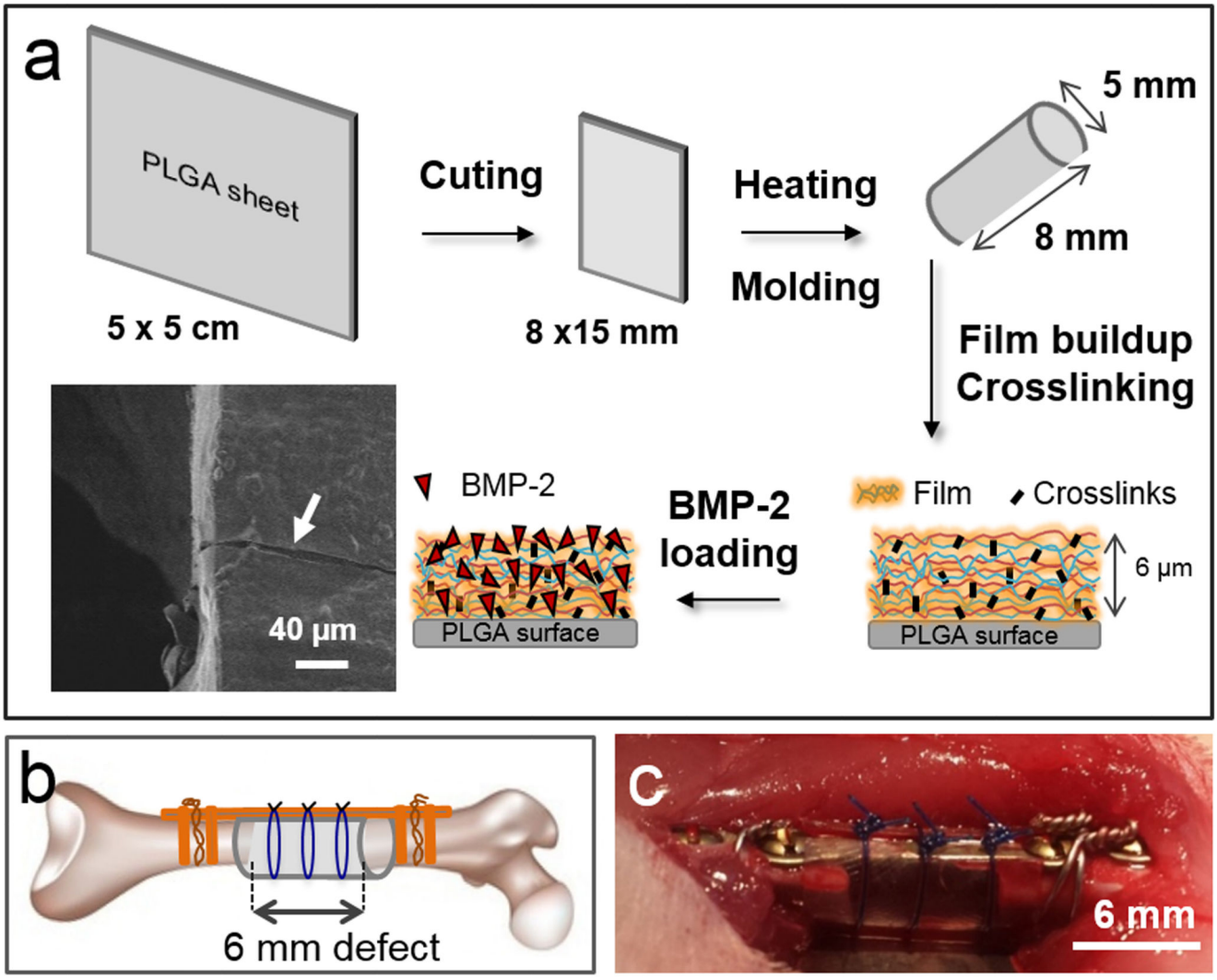

Figure 1. Experimental design of the *in vivo* experiments in rat femoral critical-size defect.

(A) Procedure for the film buildup on the PLGA membrane: the PLGA sheet is cut to the appropriate size and molded into a hollow tube. The film is built on the tube, crosslinked and post-loaded with BMP-2. The film-coated membrane can be visualized by scanning electron microscopy. Both EDC crosslinking and BMP-2 loaded amounts are adjustable parameters. A scanning electron microscopy side view of the film-coated PLGA membrane reveals the presence of the film after scratching (white arrow). (B) Scheme of the critical defect with the PLGA membrane shaped as a hollow tube and fixed with external fixators (plate and screws) and suture wires. (C) Post-operative view of the implanted PLGA tube maintained by suture wires.

A

EDC	10	30	70
$[BMP\text{-}2]_i$	Γ_i (µg)		
5	1.6 ± 0.3	1.0 ± 0.3	1.3 ± 0.3
25	7.3 ± 0.3	6.8 ± 0.8	7.0 ± 0.5
50	15.1 ± 0.5	15.1 ± 0.5	15.3 ± 0.8
100	29.4 ± 0.8	23.7 ± 0.8	34.6 ± 0.8

EDC	10	30	70
$[BMP\text{-}2]_i$	% rel		
5	80.7 ± 12.7	20.6 ± 2.8	0.0 ± 0.7
25	88.5 ± 8.2	45.4 ± 4.0	14.5 ± 0.8
50	90.4 ± 7.2	51.7 ± 5.3	19.0 ± 1.5
100	91.0 ± 1.5	51.8 ± 7.2	22.3 ± 1.9

EDC	10	30	70
$[BMP\text{-}2]_i$	Γ_R (µg)		
5	1.3 ± 0.3	0.3 ± 0.3	0.0 ± 0.3
25	6.5 ± 0.3	3.1 ± 0.3	1.0 ± 0.3
50	13.5 ± 0.5	7.8 ± 0.5	2.9 + 0.5
100	26.8 ± 0.8	12.2 ± 0.8	7.8 ± 0.8

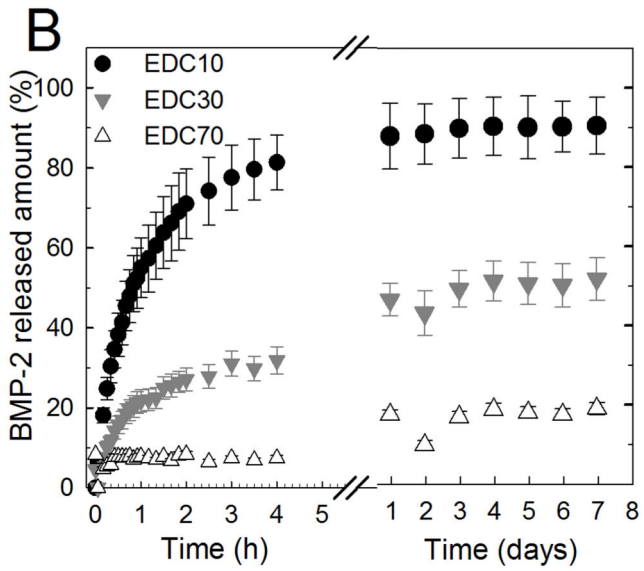

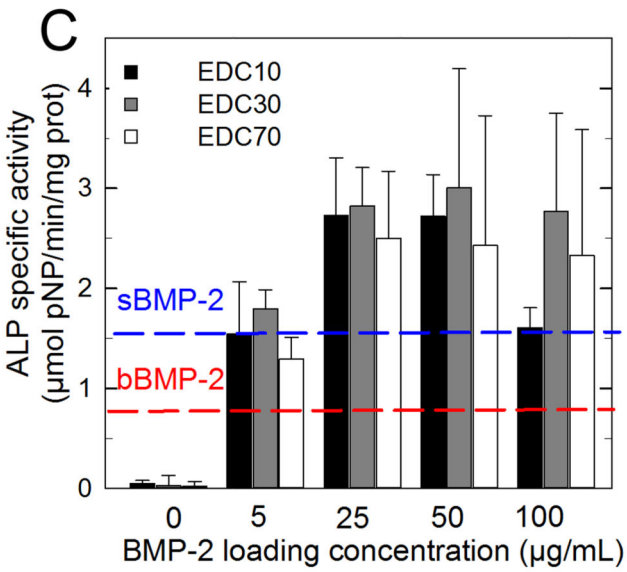

Figure 2. *In vitro* evaluation of BMP-2 loading, release and bioactivity as functions of BMP-2 initial loading concentration and film crosslinking extent (EDC).

(A) BMP-2 incorporated amounts (Γ_I,µg), % of BMP-2 released and released amount remaining after 7 days of *in vitro* release (Γ_R, µg) as a function of the initial BMP-2 concentration in the loading solution and for different crosslinker concentrations (EDC10, 30 and 70). (B) BMP-2 release profiles in physiological buffer as a function of time over 8 days, depending on the film cross-linking extent. Data represent the means ± SEM of 3 experiments. (C) *In vitro* ALP bioactivity of BMP-2-loaded films coated on PLGA membranes. Two controls were performed: BMP-2 adsorbed onto a bare PLGA membrane (red line "bBMP-2) and BMP-2 added in the GM for cells seeded directly on bare PLGA membranes (blue line "sBMP-2). Data represent the means ± SEM of 2 experiments (3 samples per experimental condition).

Europe PMC Funders Author Manuscripts

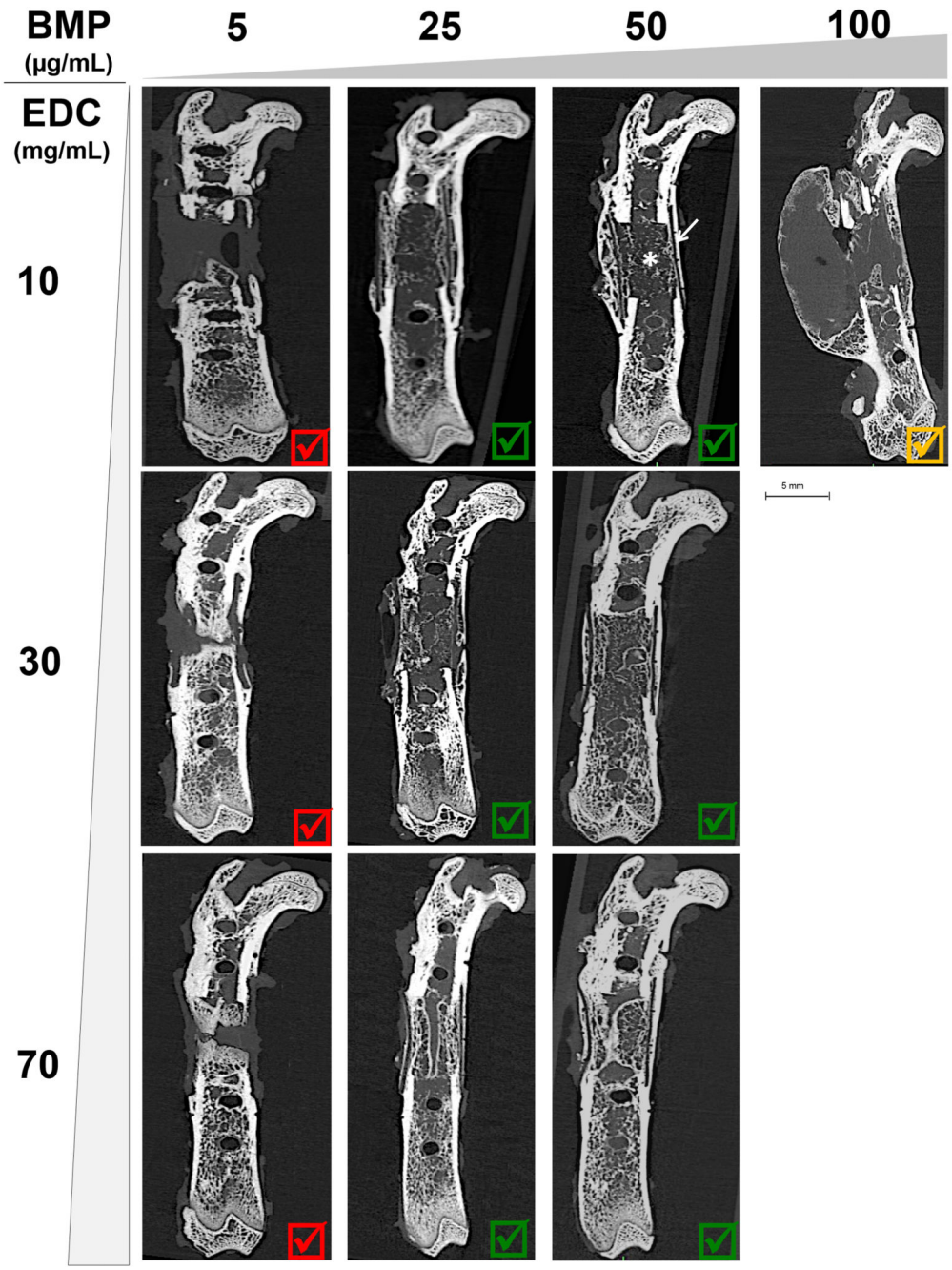

Figure 3. CµCT images at 8 weeks obtained for increasing EDC crosslinking (EDC10, EDC30 and EDC70) and BMP-2 doses from 5 to 100 µg/mL.

Sagittal cross-sections are shown for the 10 pre-screened conditions (see Table 1). All EDC5 conditions lead to an inappropriate bone formation and are marked by a red cross. Those that lead to a satisfactory bone regeneration are marked by a green V sign. The EDC10/BMP100 condition is marked by an orange V sign as it lead to a bone shell formation if the hematoma was not punctured.

Europe PMC Funders Author Manuscripts

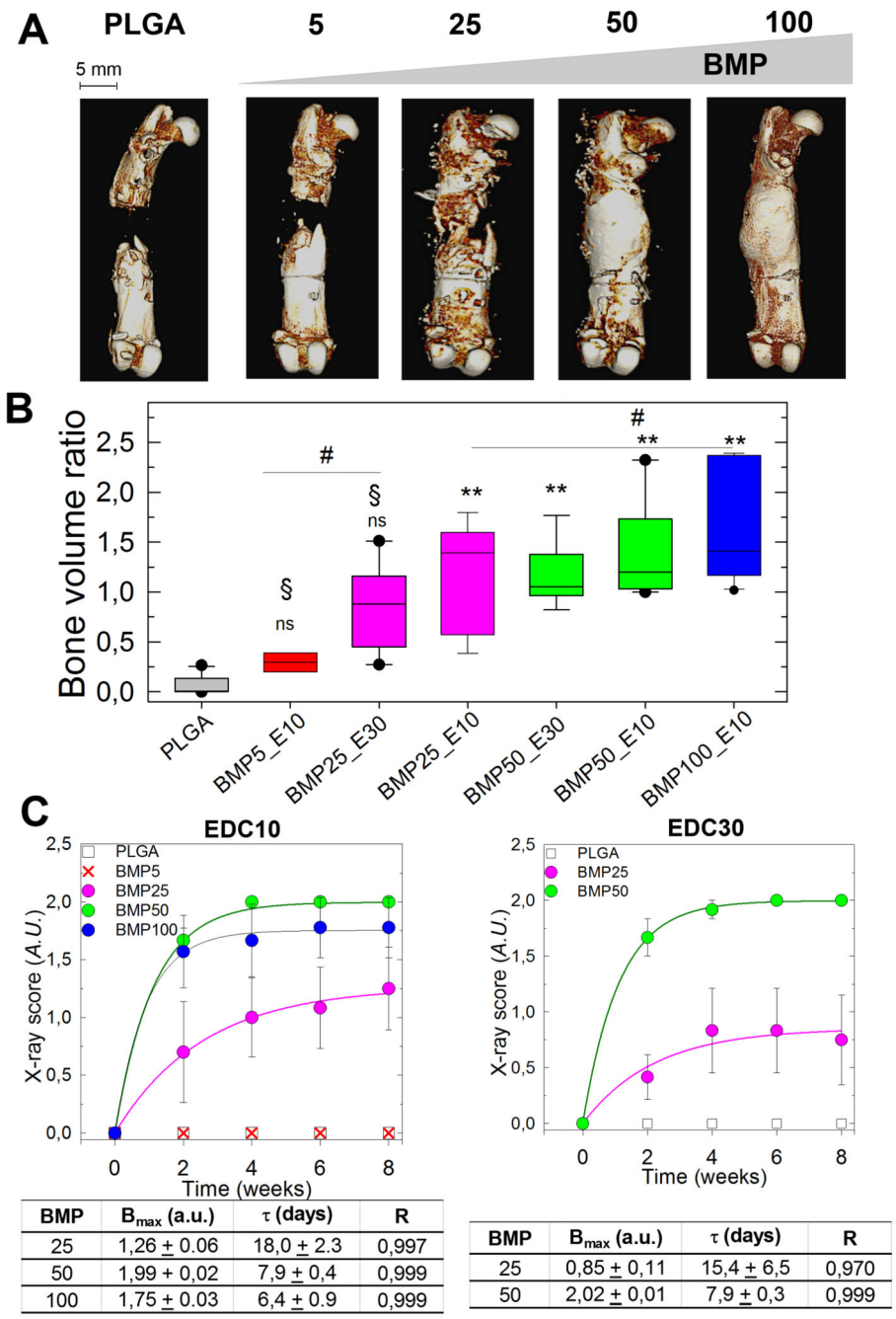

BMP	B_{max} (a.u.)	τ (days)	R
25	1,26 ± 0.06	18,0 ± 2.3	0,997
50	1,99 + 0,02	7,9 ± 0,4	0,999
100	1,75 ± 0.03	6,4 ± 0.9	0,999

BMP	B_{max} (a.u.)	τ (days)	R
25	0,85 ± 0,11	15,4 ± 6,5	0,970
50	2,02 ± 0,01	7,9 ± 0,3	0,999

Figure 4. Quantitative analysis of bone regeneration by X-ray and CμCT. Quantitative analysis of bone regeneration by X-ray and CμCT.

(A) Representative 3D CμCT reconstructions taken at 8 weeks after implantation for EDC with increasing doses of BMP-2 (BMP5 to BMP100) and control PLGA (scale bars, 5 mm). (B) Box plot representation of the bone volume ratio at 8 weeks ($n = 8$, except for BMP5/EDC10 with $n = 2$) for the EDC10 and EDC30 films with increasing BMP-2 doses from BMP5 to BMP100. BMP25 groups are in pink, BMP50 in green and BMP100 in blue (for simplification of the X-axis, the EDC is abbreviated by E). All groups were compared to the PLGA group. $*P < 0.05$, $**P < 0.01$, # indicates no significant difference between pairs, §

indicates significant difference ($P < 0.05$) compared to BMP100 group, ns indicates no significant difference compared to PLGA group (pairwise Mann-Whitney U test) (C) X-ray scores calculated from X-ray images as a function of time and corresponding exponential fits to the data (colored lines) for EDC10 (D) and EDC(30) groups. The plateau value (*Bmax)*, characteristic time τ (days) deduced from the fits and fit quality R are given in the corresponding tables.

Europe PMC Funders Author Manuscripts

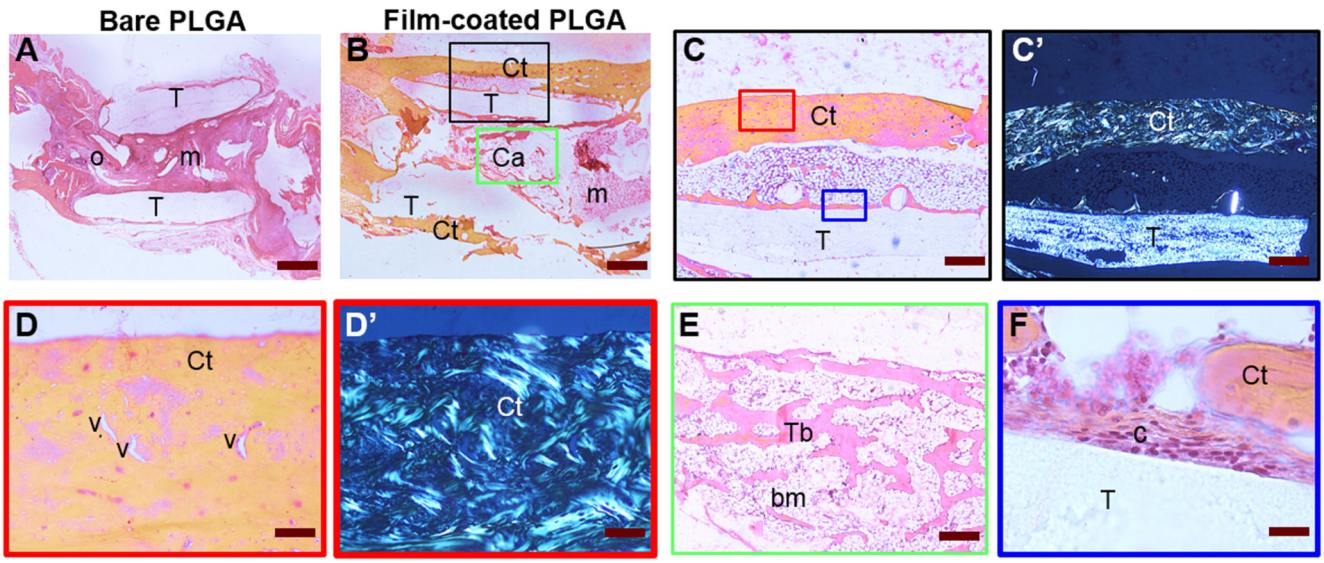

Figure 5. Histological analysis.

Representative bone tissue cross-sections of (A) control PLGA and (B) film-coated PLGA at 8 weeks post-implantation. (A) The PLGA tube (T) was found between the two femoral edges: (A) in mesenchymal tissue (m) and at the ossification point (o). In contrast (B), cortical bone (Ct) and cancellous bone (Ca) with bone marrow (bm) were found outside and inside the film-coated PLGA tube, bridging the initial defect. (C) Corresponds to a larger magnification of the black box in (B); (D) to a larger magnification of red box in (C) with visible blood vessels (v); (C', D') are the corresponding polarized light micrographs showing the birefringence of collagen strands. (E) Magnified view of trabecular bone, corresponding to green box in (B), in which bone marrow is present. (F) Magnified view of the tube/tissue interface in (C) with adhesive cells (c) observed on the film-coated PLGA. Scale bars are as follows: (A, B): 800 μm; (C, C'): 400 μm; (D, D', E): 80 μm; (F): 20 μm.

Europe PMC Funders Author Manuscripts

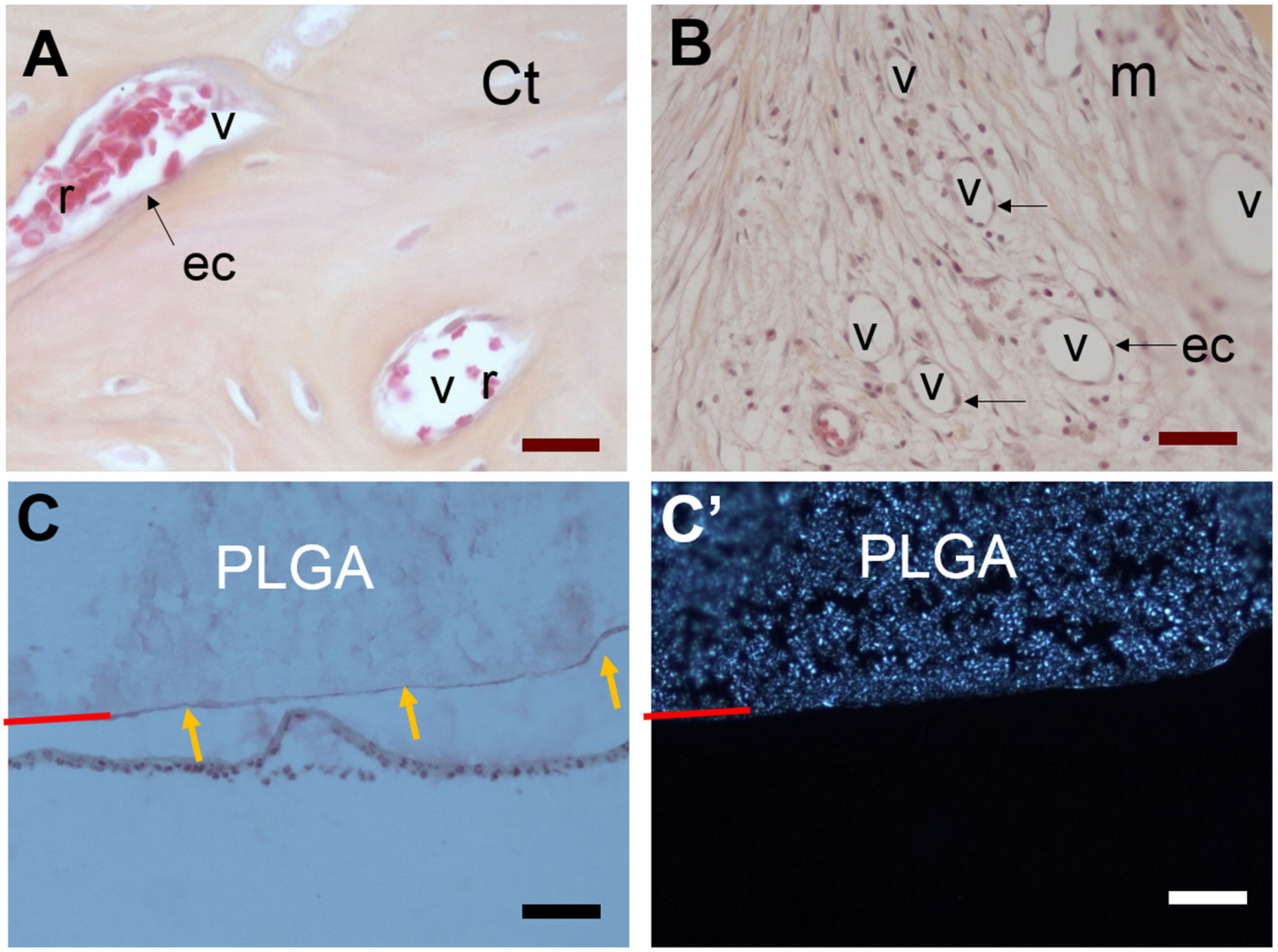

Figure 6. Histological observations of vascularization of regenerated bone tissue and of PLGA/ tissue interface.

High resolution histological observations reveals the presence of numerous vessels (v) in the regenerated bone: (A) cortical (Ct) bone and (B) mesenchymal tissue (m); The vessels (v) can clearly be identified by the presence of endothelial cells (ec, indicated by black arrows) lining along the vessel walls and by red blood cells (r) with their characteristic discoidal shape and absence of nucleus. (C,C') Imaging of PLGA/tissue interface of the same zone with optical microscopy (C) and polarized light (C'). Polarized light shows the birefringence of PLGA, which is due to its semi-crystalline structure. The PLGA surface is indicated by a red line. To note, the PLGA surface appears diffuse when observed by polarized microscopy (C') whereas a thin continuous line is visible in (C, orange arrows). This continuous lines corresponds to the polyelectrolyte film coating at the PLGA surface (with a thickness of only few μm).

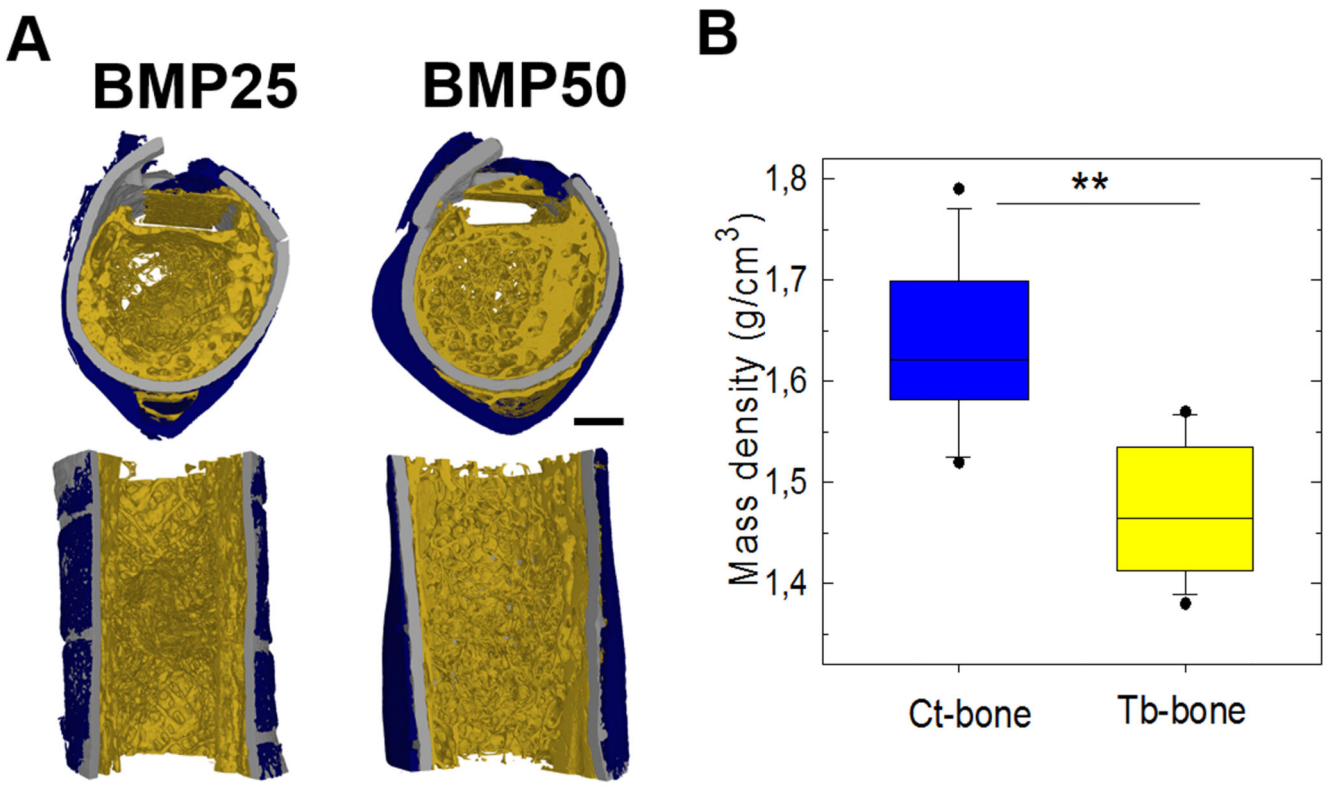

Figure 7. High-resolutiofin morphological analysis of bone regeneration using SRμCT at 8 weeks after implantation.

(A) Representative transversal and sagittal cross-sections of 3D SRμCT reconstructions of film-coated PLGA tubes at BMP-2 doses of BMP25 and BMP50 (scale bars, 1 mm). (B) Bone mass density of Ct-bone and Tb-bone as determined by SRμCT. Data are presented by boxplot for all samples pooled together, irrespective of the EDC or BMP-2 dose ($n = 12$). ** $P < 0.01$ (Wilcoxon paired test).

Europe PMC Funders Author Manuscripts

Europe PMC Funders Author Manuscripts

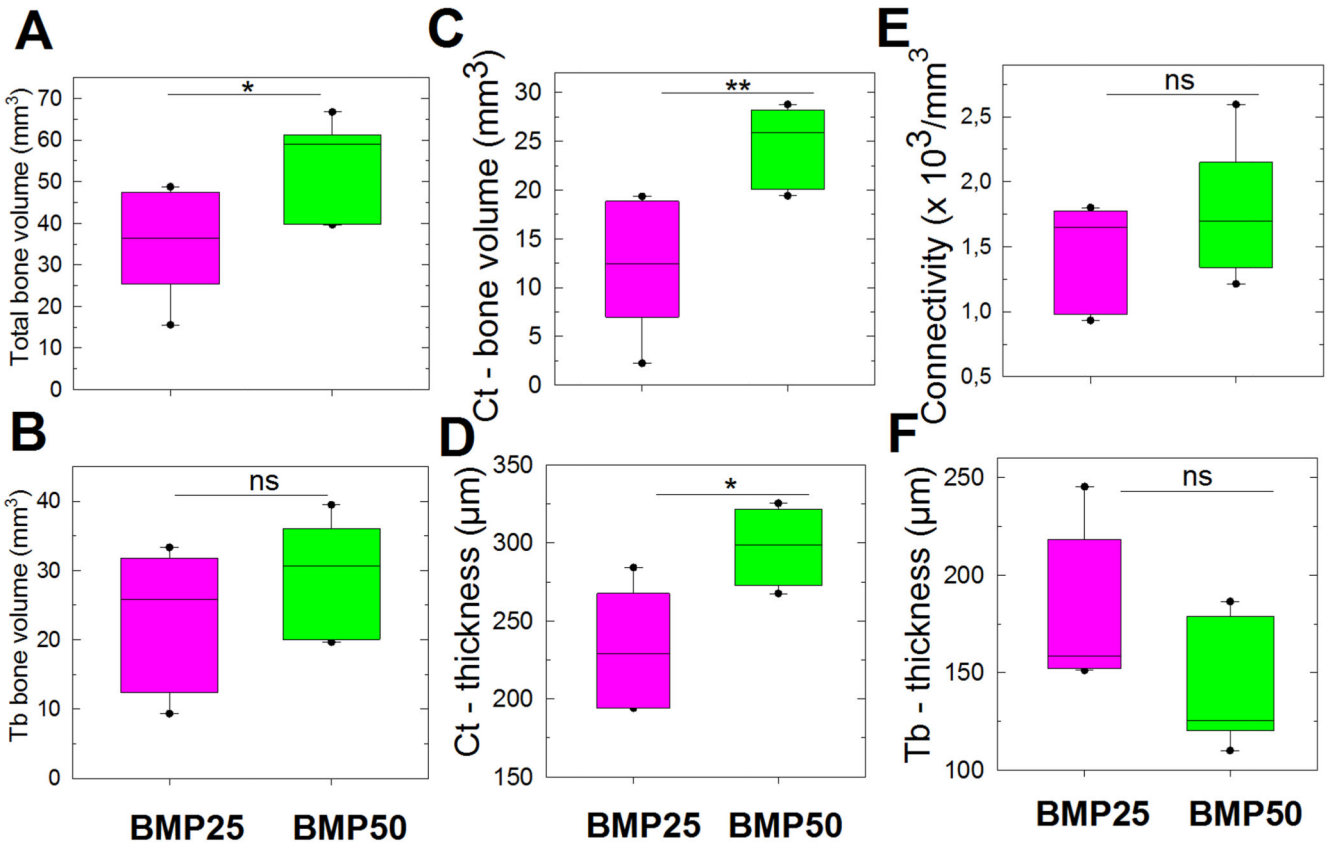

Figure 8. Bone volumes quantified using SRµCT.

Data are presented by boxplots at 8 weeks after implantation for films loaded with BMP25 or BMP50, the EDC groups being pooled together ($n = 6$ for each BMP concentration). (A) Total bone volume. (B) Tb-bone volume. (C) Ct bone volume and (D) Ct thickness. (E) Connectivity and (F) trabecular thickness in Tb bone. * $P < 0.05$, ** $P < 0.01$; *ns*, not significant (Mann-Whitney U test).

Europe PMC Funders Author Manuscripts

Table 1

Experimental conditions and total number of rat per group studied. For conditions only studied in the preliminary experiments, $n = 2$. For all the 5 selected groups in the subsequent experiment, the total number of samples per condition was $n = 8$. In addition to these BMP-containing conditions, two negative control groups were added: i) defect left with no implant to confirm the critical size of the defect (no PLGA tube, $n = 3$) and ii) bare PLGA ($n = 8$).

Parameter **Crosslinking**	**BMP-2 concentration in the loading solution (μg/mL)**			
	BMP5	**BMP25**	**BMP50**	**BMP100**
EDC10	2	2+6	2+6	2+6
EDC30	2	2+6	2+6	-
EDC70	2	2	2	-
Control **Ads BMP-2 on bare PLGA**		2	2	2

Europe PMC Funders Author Manuscripts

Table 2

Presence of clinical hematoma, punctured hematoma and percentage of bone defects that were completed healed in the case of the bare PLGA, EDC10 groups with increasing concentrations of BMP-2 from BMP5 to BMP100 and EDC30 groups at BMP25 and BMP50. (n=8 for all groups expect for the BMP-2 group n=2). (m) indicates a minimal clinical hematoma, which thus was not punctured.

Groups	Clinical Hematoma	Punctured Hematoma	Complete bone healing
Bare PLGA	0%	0	0%
EDC10 groups			
BMP5 (n=2)	0%	0	0%
BMP25	0%	0	62.5 %
BMP50	12.5% (m)	0	100%
BMP100	75 %	6	100%
EDC30 groups			
BMP25	12.5% (m)	0	50%
BMP50	0%	0	100%